Plane Wave Scattering by a Moving PEC Circular Cylinder

Eliran Mizrahi and Timor Melamed, *Member, IEEE*

***Abstract*— This paper is concerned with the scattering of a time-harmonic electromagnetic (EM) plane wave (PW) by a fast and slow moving perfectly electric conducting circular cylinder under the framework of Einstein's special relativity. By applying the Lorentz and EM field transformations to the scatterer comoving frame of reference, the problem is mapped into a PW scattering from a stationary cylinder. By using the well-known (stationary cylinder) exact and asymptotic solutions, we obtain the scattered EM field in this frame. These fields are then mapped back to the incident-field frame of reference. This procedure yields the exact and asymptotic scattered EM fields. We discuss several relativistic wave phenomena such as shifted shadow regions, velocity-dependent incident, and reflection angles and velocity-dependent creeping waves to name a few. Finally, we apply a low-speed approximation to the wave potentials and discuss the corresponding wave phenomena.**

***Index Terms*— Canonical problems, low-speed approximation (LSA), scattering from moving objects, special relativity.**

I. Introduction

In this contribution, we address the canonical problem of a time-harmonic (TH) plane wave (PW) scattering from a fast moving perfectly electric conducting (PEC) circular cylinder. The special case of a *stationary* cylinder is considered as a canonical problem as it reveals a fundamental wave phenomenon, the creeping wave. The asymptotic solution that is obtained has been used for generalizing the excitation mechanism and propagation for the generic solution of a smooth convex surface diffraction (see [1] and references therein). The scattering of an electromagnetic (EM) PW by a moving PEC cylinder was considered in [2] and included an investigation of the equiphase and equimagnitude surfaces and of the Doppler frequency shift effect. The Fourier spectrum of PW scattering by PEC and dielectric cylinders in translational motion was evaluated in [3]. Fourier analysis of the scattering by 3-D objects in translational motion was investigated in [4] and [5] by applying a vector and a scalar potential to the sources at rest. PW decomposition of the incident field has been formulated and applied to the 2-D problem of the scattering of a Gaussian beam from a fast moving perfectly conducting cylinder in [6]. It has also been used in [7] for solving the EM field that is radiated by an infinitely long thin wire antenna which uniformly translates in a direction parallel to a plane interface. Other recent contributions to relativistic scattering can be found in [8]–[14].

Manuscript received November 3, 2017; revised March 26, 2018; accepted April 4, 2018. Date of publication April 13, 2018; date of current version July 3, 2018. *(Corresponding author: Timor Melamed.)*

The authors are with the Department of Electrical and Computer Engineering, Ben-Gurion University of the Negev, Beer Sheva 84105, Israel (e-mail: timormel@bgu.ac.il).

Color versions of one or more of the figures in this paper are available online at http://ieeexplore.ieee.org.

Digital Object Identifier 10.1109/TAP.2018.2826654

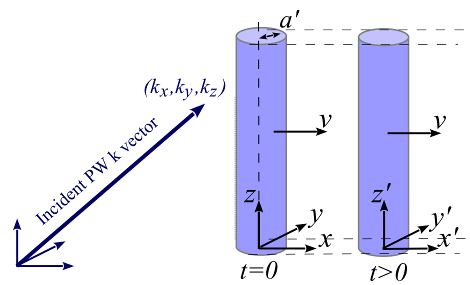

Fig. 1. Physical configuration. An incident PW is impinging on a circular cylinder of radius a' that translates uniformly along the x-axis.

Though a formal solution for PW scattering from a moving PEC circular cylinder exists in the literature, no through investigation was conducted in order to obtain a geometrical theory of diffraction (GTD) solution that is adjusted for the scatterer velocity. The present contribution is aimed at obtaining the large moving cylinder scattering and investigating the associated wave phenomena. The interpretation of the scattering of a canonical problem in the incident-field frame shed light on basic wave phenomena and can eventually lead to direct methods in that frame. Such methods can also be used for solving the scattering of bodies moving with different speeds or for bodies moving (slowly) and rotating in which local interactions that include multiple scattering may arise. The canonical problem of PW scattering can be extended for a wider class of problems by applying PW spectral decomposition of the incident field and using the results in this paper for each spectral PW scattering.

II. Problem Definition

We aim at obtaining the exact and asymptotic scattered fields from a PEC circular cylinder that translates uniformly in vacuum (see Fig. 1). The incident EM PW is given as

$$\begin{aligned}\mathbf{E}(\mathbf{r},t) &= \mathbf{E}_0 \exp(-j\mathbf{k}\cdot\mathbf{r})\exp(j\omega t)\\ \mathbf{H}(\mathbf{r},t) &= \mathbf{H}_0 \exp(-j\mathbf{k}\cdot\mathbf{r})\exp(j\omega t)\end{aligned} \tag{1}$$

where $\mathbf{r}=(x,y,z)$ are the Cartesian coordinates, the amplitudes $\mathbf{E}_0$ and $\mathbf{H}_0$ are given as

$$\mathbf{E}_0 = E_{0x}\mathbf{u}_x + E_{0y}\mathbf{u}_y + E_{0z}\mathbf{u}_z, \quad \mathbf{H}_0 = (k\eta_0)^{-1}\mathbf{k}\times\mathbf{E}_0 \tag{2}$$

0018-926X © 2018 IEEE. Personal use is permitted, but republication/redistribution requires IEEE permission.
See http://www.ieee.org/publications_standards/publications/rights/index.html for more information.

where $\eta_0 = \sqrt{\mu_0/\varepsilon_0}$ denotes the free-space impedance with ε_0 and μ_0 being the permittivity and permeability of vacuum, respectively, and $\mathbf{k}\cdot\mathbf{E}_0 = 0$. Here and throughout, unit vectors are denoted by boldfaced $\mathbf{u}$ with the appropriate subscript. In (1), $\mathbf{k} = [k_x(k_z, k_y), k_y, k_z]$ is the wavenumber vector with

$$k_x(k_z, k_y) = \sqrt{k^2 - k_y^2 - k_z^2}, \quad \mathrm{Re}k_x \geq 0, \ \mathrm{Im}k_x \leq 0 \tag{3}$$

being the longitudinal wavenumber, where $k = \omega/c$. We assume that the incident PW is propagating, i.e., $k^2 > k_y^2 + k_z^2$. Note that in (1), we have kept the $\exp(j\omega t)$ time dependence explicitly. This enables the application of the Lorentz transformation (LT) to the incident field. We refer to the $(\mathbf{r}, ct)$ frame as the *incident-field frame*.

Without the loss of generality, we choose the cylinder velocity that is denoted by $\mathbf{v}$ to be $\mathbf{v} = \upsilon\mathbf{u}_x$, where $0 \leq \upsilon < c$ is the cylinder speed. At time $t = 0$, the cylinder axis is located at $x = y = 0$. We refer to the comoving $(\mathbf{r}', ct')$ frame that is moving in $\mathbf{v}$ relatively to the incident-wave frame, as the *cylinder frame*. The cylinder is infinite along the z'-axis and is of radius a' (in the cylinder comoving frame). Quantities in the cylinder frame are denoted by a prime.

The cylinder frame boundary conditions are given by

$$E'_{z'}(\mathbf{r}', t') = 0, \quad E'_{\phi'}(\mathbf{r}', t') = 0 \quad \text{at} \quad \rho' = a' \tag{4}$$

where $\mathbf{E}'$ denotes the electric field in the cylinder frame, and ρ' and ϕ' are the conventional cylindrical coordinates.

III. Fields in the Cylinder Frame

The evaluation of EM fields that are scattered by objects in uniform motion is carried out under the framework of Einstein's theory of special relativity. In the special case of $\mathbf{v} = \upsilon\mathbf{u}_x$, the LT takes the form of

$$t' = \gamma(t - \beta x/c), \quad x' = \gamma(x - c\beta t), \ y' = y, \ z' = z \tag{5}$$

where c denotes the speed of light in vacuum and

$$\beta = \upsilon/c, \quad \gamma = 1/\sqrt{1-\beta^2}. \tag{6}$$

By using the vacuum constitutive relations, the corresponding EM field transformation (FT) is given as

$$\begin{aligned} E'_x &= E_x, \quad E'_y = \gamma(E_y - \beta\eta_0 H_z), \ E'_z = \gamma(E_z + \beta\eta_0 H_y)\\ H'_x &= H_x, \quad H'_y = \gamma\left(H_y + \frac{\beta E_z}{\eta_0}\right), \ H'_z = \gamma\left(H_z - \frac{\beta E_y}{\eta_0}\right). \end{aligned} \tag{7}$$

The inverse LT (ILT) and the inverse FT are obtained by interchanging in (5) and in (7), the primed and unprimed constituents and substituting υ with $-\upsilon$.

By applying the LT and FT in (5)–(7) to the incident PW in (1), the incident field in the *cylinder frame* is identified as the PW

$$\begin{aligned} \mathbf{E}'(\mathbf{r}', t') &= \mathbf{E}'_0 \exp(-j\mathbf{k}'\cdot\mathbf{r}')\exp(j\omega' t')\\ \mathbf{H}'(\mathbf{r}', t') &= \mathbf{H}'_0 \exp(-j\mathbf{k}'\cdot\mathbf{r}')\exp(j\omega' t') \end{aligned} \tag{8}$$

where $\mathbf{E}'_0$ and $\mathbf{H}'_0$ are related to $\mathbf{E}_0$ and $\mathbf{H}_0$ via (7) and

$$\mathbf{k}' = (k'_x, k_y, k_z), \quad \omega' = \gamma(\omega - k_x\upsilon) \tag{9}$$

with $k'_x = \gamma(k_x - k\beta)$, are identified as the wavenumber and frequency in the cylinder frame, respectively.

A. Exact Spectral Solution

In order to obtain the exact scattered EM fields, we express the total EM fields in the form of the Hertz potentials with Lorentz gauge. For a cylindric scattering problem, the magnetic potential $\mathbf{A}$ and the electric potential $\mathbf{F}$ are chosen to be directed along the z-(cylinder)axis, that is

$$\mathbf{A}'(\mathbf{r}', t') = \Psi_a'^{(t)}(\mathbf{r}', t')\mathbf{u}_z, \quad \mathbf{F}'(\mathbf{r}', t') = \Psi_f'^{(t)}(\mathbf{r}', t')\mathbf{u}_z. \tag{10}$$

The TM or TE fields are obtained from the $\mathbf{A}'$ or $\mathbf{F}'$ Hertz potentials, respectively, via the differential operators in [15].

The *total* Hertz potentials due to the incident PW in (8) subject to the boundary conditions in (4) are given as [15]

$$\begin{aligned} \Psi_{a/f}'^{(t)}(\mathbf{r}', t') &= \Psi_{a/f}'^{0}\exp(-jk_z z')T_{a/f}'^{(t)}(\varphi', \rho')\exp(j\omega' t')\\ \Psi_a'^{0} &= j\omega'\varepsilon_0 E'_{0z}/k_\rho'^{2}, \quad \Psi_f'^{0} = j\omega'\mu_0 H'_{0z}/k_\rho'^{2} \end{aligned} \tag{11}$$

where ω' is given in (9)

$$\varphi' = \phi' - \phi'_k \tag{12}$$

and the transverse vector wavenumber in cylindrical coordinates, (k'_ρ, ϕ'_k), is related to $\mathbf{k}'$ in (9) via

$$k'_x = k'_\rho\cos\phi'_k, \quad k'_y = k'_\rho\sin\phi'_k. \tag{13}$$

In (11), $T_{a/f}'^{(t)}(\varphi', \rho')$ are given by the well-known series of Bessel and Hankel functions in [15, eqs. (5–107), (5–115)].

B. Asymptotic Solution for Large Scatterers

In this section, we review the special case of high-frequency excitation in which the cylinder radius is large on the scale of the transverse wavenumber, i.e., for $k'_\rho a' \gg 1$. These asymptotic solutions are used in Section V to explore different wave phenomena in the incident-field frame that are related to the scatterer velocity. Following the standard GTD analysis in [1], the total field asymptotic terms are presented as a sum of incident, reflected, and creeping-wave terms in the form

$$\begin{aligned} T_{a/f}'^{(t)} \sim \big[T_{a/f}'^{(i)} + T_{a/f}'^{(r)} - T_{a/f(0)}'^{(c)[-\mathrm{sgn}(\varphi')]}\big]U[\zeta'(\mathbf{r}')]\\ + \sum_{m=0}^{\infty}\big[T_{a/f(m)}'^{(c)(+)} + T_{a/f(m)}'^{(c)(-)}\big] \end{aligned} \tag{14}$$

in which the Heaviside function, $U()$, with

$$\zeta'(\mathbf{r}') = |\varphi'| - \pi/2 + \cos^{-1}(a'/\rho') \tag{15}$$

restricts the contributions of the first three terms in (14) to the light region that is defined by $\zeta'(\mathbf{r}') > 0$. In (14), we identify

$$T_a'^{(i)} = T_f'^{(i)} = \exp\big[-jk'_\rho L'^{(i)}(\rho', \varphi')\big] \tag{16}$$

with

$$L'^{(i)}(\rho', \varphi') = \rho'\cos\varphi' \tag{17}$$

as the *incident* wave terms. The *reflected* field terms that are denoted by the superscript (r) are given as

$$\begin{aligned} T_f'^{(r)} = -T_a'^{(r)} &= \sqrt{\frac{R'^{(r)}}{L'^{(r)}(\rho') + R'^{(r)}}}\\ &\times \exp\big[-jk'_\rho L'^{(i)}(a', \pi - \delta') - jk'_\rho L'^{(r)}(\rho', \varphi')\big] \end{aligned} \tag{18}$$

where $L'^{(i)}$ is given in (17) and

$$L'^{(r)}(\rho',\varphi') = \sqrt{\rho'^2 - a'^2\sin^2\delta'} - a'\cos\delta'$$
$$R'^{(r)}(\rho',\varphi') = a'\cos\delta'/2. \tag{19}$$

Here, the angle δ' is obtained by solving

$$\cos^{-1}\left(-\frac{a'\sin\delta'}{\rho'}\right) - 2\left(\delta' + \frac{\pi}{2}\right) + |\varphi'| - \frac{\pi}{2} = 0. \tag{20}$$

Finally, the *creeping*-wave terms in (14), which are denoted by the superscript (c), are given as

$$T'^{(c)(\pm)}_{a/f(m)} = \left(\frac{k'_\rho a'}{2}\right)^{1/3} 2\exp\left(-j\frac{\pi}{12}\right) G[k'_\rho L'^{(c)}(\rho')]\mathbb{A}_{a/f}$$
$$\times \exp\left\{-j\nu'_{a/f}\left[\frac{\pi}{2} + 2\pi m - \cos^{-1}\left(\frac{a'}{\rho'}\right) \pm \varphi'\right]\right\} \tag{21}$$

where

$$G(kR) = \frac{\exp(-jkR)}{\sqrt{8\pi kR}}, \quad L'^{(c)}(\rho') = \sqrt{\rho'^2 - a'^2} \tag{22}$$

and

$$\mathbb{A}_a = [\dot{\mathrm{A}}\mathrm{i}(-\alpha_0)]^{-2}, \quad \mathbb{A}_f = [\dot{\alpha}_0 \mathrm{Ai}^2(-\dot{\alpha}_0)]^{-1}$$
$$\nu'_{a/f} = k'_\rho a' + \alpha_{a/f}\left(k'_\rho a'/2\right)^{1/3}\exp(-j\pi/3). \tag{23}$$

Here, Ai denotes the Airy function, $-\alpha_0$ and $-\dot{\alpha}_0$ denote the first zeros of Ai and $\dot{\mathrm{A}}\mathrm{i}$, respectively, and $\alpha_a = \alpha_0$ and $\alpha_f = \dot{\alpha}_0$. In Section V, we discuss the wave phenomena that are associated with these asymptotic terms in both frames.

IV. Fields in the Incident-Field Frame

In order to obtain the EM field in the incident-field frame, we first evaluate the EM fields in the cylinder frame by applying the differential operators in [15] to the total potentials in (11). Then, in order to use the FT, we apply a cylindrical-to-Cartesian transformation to the resulting fields. Finally, we apply the inverse FT to the cylinder frame fields and sample the resulting incident-field frame fields at the corresponding $(\mathbf{r}, t)$ event that is obtained via the LT in (5). This procedure can be recast in the form

$$\Pi(\mathbf{r},t) = \left\{\mathbf{T}'\left[\mathbf{M}'\begin{pmatrix}\Psi'^{(t)}_a(\mathbf{r}',t')\\ \Psi'^{(t)}_f(\mathbf{r}',t')\end{pmatrix}\right]\right\}\Bigg|_{\begin{cases}\mathbf{r}'(\mathbf{r},t)\\ t'(\mathbf{r},t)\end{cases}} \tag{24}$$

where the vector fields are given as

$$\Pi(\mathbf{r},t) = \left[E_x, E_y, E_z, H_x, H_y, H_z\right]^T \tag{25}$$

$$\mathbf{T}' = \begin{bmatrix} C'_\phi & -S'_\phi & 0 & 0 & 0 & 0\\ \gamma S'_\phi & \gamma C'_\phi & 0 & 0 & 0 & \Upsilon'_\mu\\ 0 & 0 & \gamma & -\Upsilon'_\mu S'_\phi & -\Upsilon'_\mu C'_\phi & 0\\ 0 & 0 & 0 & C'_\phi & -S'_\phi & 0\\ 0 & 0 & -\Upsilon'_\varepsilon & \gamma S'_\phi & \gamma C'_\phi & 0\\ \Upsilon'_\varepsilon S'_\phi & \Upsilon'_\varepsilon C'_\phi & 0 & 0 & 0 & \gamma \end{bmatrix} \tag{26}$$

with $\Upsilon'_\mu = \gamma\upsilon\mu_0$, $\Upsilon'_\varepsilon = \gamma\upsilon\varepsilon_0$, $S'_\phi = \sin\phi'$, $C'_\phi = \cos\phi'$, and

$$\mathbf{M}' = \begin{bmatrix} -k_z/\left(\omega'\epsilon_0\right)\partial_{\rho'} & -\rho'^{-1}\partial_{\phi'}\\ -k_z/\left(\omega'\epsilon_0\rho'\right)\partial_{\phi'} & \partial_{\rho'}\\ k'^2_\rho/\left(j\omega'\epsilon_0\right) & 0\\ \rho'^{-1}\partial_{\phi'} & -k_z/\left(\omega'\mu_0\right)\partial_{\rho'}\\ -\partial_{\rho'} & -k_z/\left(\omega'\mu_0\rho'\right)\partial_{\phi'}\\ 0 & k'^2_\rho/\left(j\omega'\mu_0\right) \end{bmatrix}. \tag{27}$$

Note that the *asymptotic* EM fields are obtained by inserting the potentials of (11) with the asymptotic terms in (14) into (24), and then collecting the higher order k'-terms.

An alternative way to evaluate the incident-field frame EM fields is to apply the ILT to the cylinder frame *potentials*, and then apply the incident-field frame linear differential operators that are corresponding to the operators in (27), that is

$$\Pi(\mathbf{r},t) = \mathbf{T}(\mathbf{r},\mathbf{t})\mathbf{M}(\mathbf{r},\mathbf{t})\begin{bmatrix}\Psi^{(t)}_a(\mathbf{r},t)\\ \Psi^{(t)}_f(\mathbf{r},t)\end{bmatrix} \tag{28}$$

where $\Psi^{(t)}_{a/f}(\mathbf{r},t) = \Psi'^{(t)}_{a/f}[\mathbf{r}(\mathbf{r}',t'), t(\mathbf{r}',t')]$ are referred to in this paper as the *incident-field frame potentials*, $\mathbf{T}(\mathbf{r},\mathbf{t})$ is obtained by applying the LT to $\mathbf{T}'$ in (26), and the operators matrix $\mathbf{M}(\mathbf{r},\mathbf{t})$ is obtained by replacing the $\partial_{\rho'}$ and $\partial_{\phi'}$ derivatives in (27) with

$$\partial_{\rho'} = \bar{\rho}(t)^{-1}[\gamma\bar{x}(t)(\partial_x + \beta c^{-1}\partial_t) + y\partial_y]$$
$$\partial_{\phi'} = \gamma y(\partial_x + \beta c^{-1}\partial_t) - \bar{x}(t)\partial_y \tag{29}$$

where

$$\bar{\rho}(t) = \sqrt{\bar{x}^2(t) + y^2}, \quad \bar{x}(t) = \gamma(x - \upsilon t). \tag{30}$$

V. Wave Phenomena in the Incident-Field Frames

In order to explore the incident-field frame potentials, we describe a wave phenomenon in the cylinder frame, and the corresponding one in the incident-field frame.

A. Shadowing Wave

First, we consider the argument of the Heaviside function in (14) that restricts the first three terms' contributions to the total potentials $T'^{(t)}_{a/f}$ to the light region. The *shadow region* is obtained by setting $\zeta' < 0$. It follows from (15) that:

$$|\varphi'| < (\pi/2) - \cos^{-1}(a'/\rho'). \tag{31}$$

In order to interpret this condition, we define the angles

$$\theta'_\mp = \pi/2 - \cos^{-1}(a'/\rho') \mp \varphi'. \tag{32}$$

The condition in (31) sets both angles θ'_- and θ'_+ to be positive. This condition defines the (cylinder frame) *shadow region* as the area between the two parallel tangent rays [1, Fig. 3.15].

In order to obtain the incident-field frame shadow region, we apply the LT in (5) to the condition $\zeta'(\mathbf{r}') < 0$. The resulting shadow region is given as

$$\left|\tan^{-1}\left(\frac{y}{\bar{x}(t)}\right) - \phi'_k\right| - \frac{\pi}{2} + \cos^{-1}\left(\frac{a'}{\bar{\rho}(t)}\right) < 0 \tag{33}$$

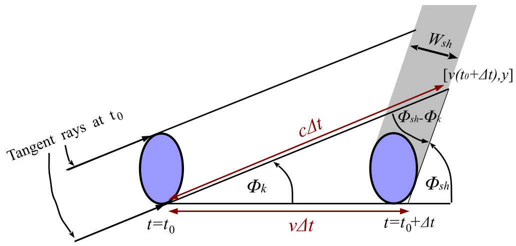

Fig. 2. Physical interpretation of the shift in the incident-field frame shadow region from the incident wave direction.

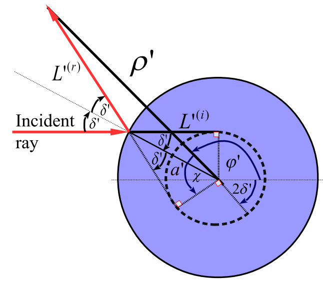

Fig. 3. Geometrical representation of Snell's law and the optical lengths.

where ϕ_k' is defined in (13). By using (9) in (13), the spectral angle ϕ_k' can be recast in terms of the incident-field frame spectral variables in the form

$$\tan\phi_k' = [k_y/k]/[\gamma\,(k_x/k - \beta)]. \tag{34}$$

By inserting the time-dependent coordinate $\bar{x}(t)$ in (30) into (33), the shadow region condition takes the form

$$|\bar{\varphi}(t)| < \pi/2 - \cos^{-1}[a'/\bar{\rho}(t)] \tag{35}$$

where $\bar{\rho}(t)$ is given in (30) and

$$\bar{\varphi}(t) = \tan^{-1}[y/\bar{x}(t)] - \phi_k'. \tag{36}$$

By comparing (35) with (31), we note that these conditions have essentially the same form. Thus, in the $[\bar{x}(t), y]$ system, the shadow is casted in the direction of ϕ_k' and has a width of $2a'$. It follows that in the incident-field frame, the shadow is casted in the direction of the angle ϕ_{sh} that is defined by

$$\tan\phi_{\mathrm{sh}} = \frac{\Delta y}{\Delta(x - \upsilon t)} = \gamma\,\tan\phi_k'. \tag{37}$$

Note that the incident-field frame shadow angle ϕ_{sh} is measured relatively to the x-axis in the Galilean system $(x - \upsilon t, y)$. Thus, the shadow region translates uniformly with the cylinder (see Fig. 2). Furthermore, unlike the stationary $\beta = 0$ case, the shadow angle, ϕ_{sh}, exhibits a shift from the incident-field angle ϕ_k. By using $\sin\phi_k = k_y/k$ in (34) and inserting into (37), we obtain

$$\tan\phi_{\mathrm{sh}} = \frac{\sin\phi_k}{\cos\phi_k - \beta}. \tag{38}$$

The shift of the shadow boundaries direction from ϕ_k (stationary cylinder) to (the moving cylinder) ϕ_{sh} in (38) has a clear physical interpretation. Referring to Fig. 2, we examine the cylinder in the incident-field frame at certain time t_0 at which the cylinder is located at some point over the x-axis (the left cylinder in Fig. 2). At that time, the incident-field front is impinging on the cylinder and propagates into the light region with angle ϕ_k. In Fig. 2, the two tangent rays are plotted. After certain time $\Delta t > 0$, the cylinder has advanced a distance of $\upsilon\Delta t$ (the right-hand side cylinder in Fig. 2), whereas the wavefront of the grazing rays have propagated a distance of $c\Delta t$. At this time, a new wavefront is formed by the incident grazing rays with angle ϕ_k.

Thus, the light to shadow transition occurs over the current $(t + \Delta t)$ cylinder tangent that passes through the incident-field front at $t + \Delta t$ as plotted in Fig. 2. This tangent forms an angle of ϕ_{sh} with the x-axis. By applying the sine theorem to the plotted triangle, we deduce that

$$\frac{\upsilon\Delta t}{\sin(\phi_{\mathrm{sh}} - \phi_k)} = \frac{c\Delta t}{\sin\phi_{\mathrm{sh}}}. \tag{39}$$

By using β in (6) as well as basic trigonometry for $\sin(\phi_{\mathrm{sh}} - \phi_k)$, we end up with the result in (38).

In order to evaluate the shadow *width* that is denoted by W_{sh}, we note that in $(\bar{x}, y)$ coordinates, the shadow width is $2a'$. Therefore, the shadow boundaries are given as

$$y = \bar{x}\tan\phi_k' \pm a'/\cos\phi_k'. \tag{40}$$

By using (38) in (40), we obtain the corresponding boundaries in the incident-field frame as

$$y = (x - \upsilon t)\tan\phi_{\mathrm{sh}} \pm a'\sqrt{1 + \gamma^{-2}\tan^2\phi_{\mathrm{sh}}}. \tag{41}$$

Thus, the shadow width in the incident-field frame, which is the distance between these lines, is evaluated as

$$W_{\mathrm{sh}} = 2a'\gamma^{-2}\cos\phi_{\mathrm{sh}}\sqrt{\gamma^2 + \tan^2\phi_{\mathrm{sh}}} \tag{42}$$

where ϕ_{sh} is given in (38). The shadow boundaries and the shadow width are plotted in Fig. 2.

B. Reflected Potentials

The reflected wave term in (18) results from the contribution of a stationary point in the Watson transformation integral [1]. The stationary point that is denoted by ν_s^- is given as

$$\nu_s^- = k_\rho' a' \cos(\delta' + \pi/2) \tag{43}$$

where the angle δ' is obtained by solving (20). In order to interpret the wave phenomenon that is associated with the reflected wave, we recast (20) in the form

$$-2\delta' = 2\pi - (\chi' + |\varphi'| + \pi/2) \tag{44}$$

where $\chi' = \cos^{-1}[a'\sin(-\delta')/\rho']$. This relation can also be derived from the geometrical representation of Snell's law by setting both the incident and reflection angles to δ' as demonstrated in Fig. 3.

Referring to Fig. 3, we identify $L'^{(i)}$ in (17) as the optical length of the *incident* ray that is impinging on the cylinder surface and that is propagating to the observation point with a reflection angle that is equal to the incident angle δ'. The $L'^{(r)}$ term in (19) is identified as the optical length of the *reflected* ray from the scatterer surface to the observation point.

By applying simple geometry to the triangles in Fig. 3, we deduce that the optical length of the reflected ray trajectory over the xy plane is given by $L'^{(i)}(a', \pi - \delta') + L'^{(r)}(\rho', \phi')$ where $L'^{(r)}$ is given by (19), and by using (17), we identify

$$L'^{(i)}(a', \pi - \delta') = a' \cos(\pi - \delta'). \quad (45)$$

By inserting (18) into (11), we obtain the asymptotic reflected potentials of the 3-D problem as

$$\Psi'^{(r)}_{a/f}(\mathbf{r}', t') \sim \Psi'^{(i)}_{\rm ray} \Psi'^{(r)}_{\rm ray} \quad (46)$$

in which

$$\Psi'^{(i)}_{\rm ray} = \Psi'^{0}_{a/f} \exp\left(-jk_z z'_{ip}\right) \exp\left(-jk'_\rho L'^{(i)}\right) \exp\left(j\omega' t'_{ip}\right) \quad (47)$$

is identified as the incident-field potential that is sampled at the reflection event, and

$$\Psi'^{(r)}_{\rm ray} = (-1)\sqrt{\frac{R'^{(r)}}{L'^{(r)} + R'^{(r)}}} \exp\left[-jk_z\left(z' - z'_{ip}\right)\right] \times \exp\left(-jk'_\rho L'^{(r)}\right) \exp\left[j\omega'\left(t' - t'_{ip}\right)\right] \quad (48)$$

is the asymptotic reflected potential. Here, $L'^{(r)}$ and $R'^{(r)}$ are given in (19) and z'_{ip}, t'_{ip} are identified as the z' and t' values of the incident ray at the incident event over the cylinder surface. The asymptotic reflected potential term, $\Psi'^{(r)}_{\rm ray}$ consists of a reflection coefficient of (-1), an amplitude term in a canonical GTD form in which $R'^{(r)}$ is the radius of curvature of the reflected ray field over the interface, and $L'^{(r)}$ is the optical length of the reflected ray field (see Fig. 3). Note that over the cylinder surface, where $L'^{(r)} = 0$, the sum $\Psi'^{(r)}_a + \Psi'^{(i)}_a = 0$ in accordance with the cylinder frame boundary conditions.

Next, we investigate the reflected potentials in the *incident-field* frame. By applying the LT to the potentials in (46)–(48), we obtain

$$\Psi^{(r)}_{a/f}(\mathbf{r}, t) \sim (-1)\sqrt{\frac{\bar{R}^{(r)}}{\bar{L}^{(r)} + \bar{R}^{(r)}}} \Psi'^{0}_{a/f} \exp(-jk_z z) \times \exp[j\omega'\gamma\,(t - \beta x/c)] \exp\left[-jk'_\rho(\bar{L}^{(r)}(\mathbf{r}, t) - a' \cos\bar{\delta})\right]. \quad (49)$$

Here

$$\bar{L}^{(r)}(\mathbf{r}, t) = \sqrt{\bar{\rho}^2 - a'^2 \sin^2\bar{\delta}} - a' \cos\bar{\delta}$$
$$\bar{R}^{(r)}(\mathbf{r}, t) = a' \cos\bar{\delta}/2 \quad (50)$$

where $\bar{\rho}$ is given in (30), and the angle $\bar{\delta}$ is obtained from the observation event $(\mathbf{r}, ct)$ by solving

$$\cos^{-1}\left(-\frac{a' \sin\bar{\delta}}{\bar{\rho}}\right) - 2\left(\bar{\delta} + \frac{\pi}{2}\right) + |\bar{\varphi}| - \frac{\pi}{2} = 0. \quad (51)$$

The reflected potentials are formed by two events: the first is the *impinging* event that is denoted by $(\mathbf{r}^{(r)}_i, t^{(r)}_i)$. At this event, the incident plane-wave is impinging on the cylinder, and forms the reflected wave that is propagating toward the *observation* event $(\mathbf{r}, t)$. Note that when the wavefront arrives at the observation point, the cylinder has advanced $v(t - t^{(r)}_i)$. In the cylinder frame, the impinging event is given as

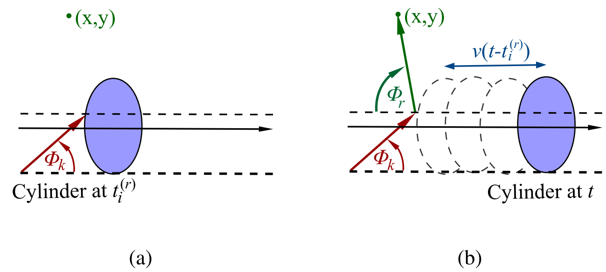

Fig. 4. Incident and reflected rays in the incident-field frame. (a) At Time $t = t^{(r)}_i$, the incident field is impinging on the moving cylinder surface. (b) At Time t, the reflected wavefront is arriving at observation point (x, y). The wave is reflected in the direction of Φ_r in (56)

$$x'^{(r)}_i = -a' \cos\delta', \quad y'^{(r)}_i = a' \sin\delta', \quad t'^{(r)}_i = t' - c^{-1} L'^{(r)} \quad (52)$$

where the cylinder frame observation event, $(\mathbf{r}', t')$ is obtained from the corresponding incident-field frame event via the LT. Thus, in terms of the observation event, the impinging event in the incident-field frame is obtained by applying the ILT to (52), giving

$$x^{(r)}_i = \gamma\,[-a' \cos\bar{\delta} + \gamma\,(\beta ct - \beta^2 x) - \beta\bar{L}^{(r)}], \quad y^{(r)}_i = a' \sin\bar{\delta}$$
$$t^{(r)}_i = \gamma\,[\gamma\,(t - \beta c^{-1} x) - c^{-1}\bar{L}^{(r)} - \beta c^{-1} a' \cos\bar{\delta}]. \quad (53)$$

A direct result of (51) is that in the time-dependent $(\bar{x}(t), y)$ coordinate system, the incident and reflection angles over the (circular) cylinder surface are both equal to $\bar{\delta}$. Therefore, in this system, the reflected ray trajectory is the line

$$y - y^{(r)}_i = -\tan\left(2\bar{\delta} - \phi'_k\right)\left(\bar{x} - \bar{x}^{(r)}_i\right) \quad (54)$$

where

$$\bar{x}^{(r)}_i = -\sqrt{a'^2 - \left(y^{(r)}_i\right)^2}. \quad (55)$$

It follows that in the (x, y) system, the ray trajectory is in the direction of the angle Φ_r that is given as

$$\tan\Phi_r = \frac{\Delta y}{\Delta(x - vt)} = \gamma\,\tan\left(2\bar{\delta} - \phi'_k\right) \quad (56)$$

where $\bar{\delta}$ is obtained by solving (51). In Fig. 4, we plot a sketch of the incident and reflected rays in the incident-field frame.

C. Creeping Wave

In order to investigate the creeping-wave phenomenon, we evaluate the creeping potentials terms, $\Psi'^{(c)(\pm)}_{a/f(m)}$ that are obtained from $T'^{(c)(\pm)}_{a/f(m)}$ by inserting (14) into (11), giving

$$\Psi'^{(c)(\pm)}_{a/f(m)}(\mathbf{r}', t') = \Psi'^{0}_{a/f} \exp(-jk_z z') \exp(j\omega' t') T'^{(c)(\pm)}_{a/f(m)} \quad (57)$$

where $T'^{(c)(\pm)}_{a/f(m)}$ are given in (21).

In order to identify the associated wave phenomenon, the following parameters are defined [1]:

$$\begin{aligned} D'_{a/f} &= \left(\frac{k'_\rho a}{2}\right)^{1/3} 2\mathbb{A}_{a/f} \exp\left(-j\frac{\pi}{12}\right) \\ \Upsilon'_{a/f} &= \frac{\alpha_{a/f}}{\sqrt[3]{2k'^2_\rho a'^2}} \exp\left(-j\frac{\pi}{3}\right) \end{aligned} \tag{58}$$

and

$$l'^m_\mp(\mathbf{r}') = a'\theta'^m_\mp, \quad \theta'^m_\mp = \frac{\pi}{2} + 2\pi m - \cos^{-1}\frac{a}{\rho'} \mp \varphi' \tag{59}$$

where φ' is given in (12). By using (58) in (23), one obtains

$$\nu'_{a/f} = a'k_\rho\left(1 + \Upsilon'_{a/f}\right). \tag{60}$$

By inserting (21) with (58)–(60) into (57), we recast $\Psi'^{(c)}_{a/f}$ in the form

$$\begin{aligned} \Psi'^{(c)(\pm)}_{a/f(m)}(\mathbf{r}', t') &= \Psi'^{(i)}_{\text{graz}}(\mathbf{r}', t') \\ &\times D'_{a/f} \exp\left[-jk'_\rho\left(1+\Upsilon'_{a/f}\right)l'^m_\mp\right] \quad G\left[k'_\rho L'^{(c)}(\rho')\right] \end{aligned} \tag{61}$$

where $L'^{(c)}$ is defined in (22), G is given in (22) and

$$\Psi'^{(i)}_{\text{graz}}(\mathbf{r}', t') = \Psi'^0_{a/f} \exp(-jk_z z') \exp(j\omega' t'). \tag{62}$$

The creeping wave potentials in (61) consist of a multiplication of several terms. The first term in (61) is identified as the sampling of the incident-field potential at the corresponding 2-D grazing point, i.e., $\Psi'^{(i)}_{\text{graz}} = \Psi'^{(i)}_{a/f}(\rho' = a', \varphi' = \pm\pi/2)$. The second term in (61) accounts for the propagation and attenuation of the creeping wave along the cylinder surface either in the clockwise (CW) ($\Psi'^{(c)(+)}_{a/f(m)}$) or counterclockwise (CCW) ($\Psi'^{(c)(-)}_{a/f(m)}$) direction. The terms l'^m_- and l'^m_+ are identified as the creeping distances along the cylinder surface from the grazing point to the emanation point of a tangential ray to the observer, plus m times the circumference of the cylinder circle. The last term in (61), $G(k'_\rho L'^{(c)})$, is identified as the tangential rays that propagate in free space to the observer (see Fig. 5).

The creeping waves encircle the cylinder an infinite number of times. In the mth round, the wave potentials accumulate a phase of $k'_\rho(1 + \text{Re}\Upsilon'_{a/f})l'^m_\mp$ and attenuate exponentially with $k'_\rho \text{Im}\Upsilon'_{a/f} l'^m_\mp$. The phase term sets its speed to be

$$v'_c = c/\left[\kappa'_\rho\left(1 + \text{Re}\Upsilon'_{a/f}\right)\right], \quad \kappa'_\rho = k'_\rho/k'. \tag{63}$$

Here, κ'_ρ denotes the (cylinder frame) incident wave normalized *lateral* wavenumber. Note that the propagation in the z' direction is accounted for the multiplication by the $\exp(-jk_z z')$ term in (22). Therefore, these waves are creeping along an *helix* contour over the circular cylinder surface. Thus, the creeping wave that is excited by the tangential ray at the grazing point $(a'\sin\phi'_k, a'\cos\phi'_k, z'_g)$ and time t_g propagates along the trajectory:

$$\mathbf{r}'_c = \left[\mp a'\sin\Phi'_c(t'), \pm a'\cos\Phi'_c(t'), z'_g + c\kappa'_z(t' - t'_g)\right] \tag{64}$$

where

$$\Phi'_c(t') = \pm\omega'_c(t' - t'_g) + \phi'_k, \quad \omega'_c = v'_c/a, \ \kappa'_z = k'_z/k'. \tag{65}$$

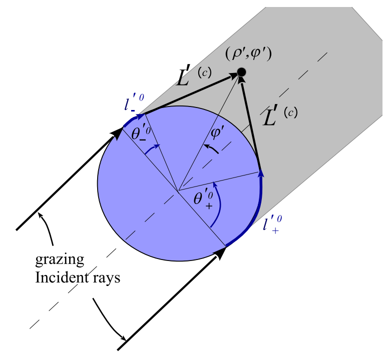

Fig. 5. Creeping wave potentials in (61) consist of sample of the incident rays at the grazing interaction points, attenuated propagation along the cylinder surface, and propagation of the tangential rays along $L'^{(c)}$ to the observation point.

The $\pm$ sign in (64) refers to either a CW (upper sign) or CCW (lower sign) trajectory.

Next, we examine the *incident-field frame* creeping wave phenomenon by applying the LT to the potentials in (61). The resulting incident-field frame potentials are given as

$$\begin{aligned} \Psi^{(c)(\pm)}_{a/f(m)}(\mathbf{r}, t) &= \Psi'^0_{a/f} \exp(-jk_z z) \exp[j\omega'\gamma(t - \beta x/c)] \\ &\times D'_{a/f} \exp\left[-jk'_\rho\left(1 + \Upsilon'_{a/f}\right)\bar{l}^m_\mp(\mathbf{r}, t)\right] G\left[k'_\rho \bar{L}^{(c)}(\mathbf{r}, t)\right] \end{aligned} \tag{66}$$

where $D'_{a/f}$ and $\Upsilon'_{a/f}$ are given in (58), G in (22) and

$$\begin{aligned} \bar{l}^m_\mp(\mathbf{r}, t) &= a'\left[\frac{\pi}{2} + 2\pi m - \cos^{-1}\frac{a'}{\bar{\rho}(t)} \mp \cos^{-1}\frac{\bar{x}(t)}{\bar{\rho}(t)} \pm \phi'_k\right] \\ \bar{L}^{(c)}(\mathbf{r}, t) &= \sqrt{\bar{\rho}^2(t) - a'^2}. \end{aligned} \tag{67}$$

Here, $\bar{x}(t)$ and $\bar{\rho}(t)$ are given in (30).

First, we examine the creeping wave trajectory over the moving cylinder surface. By applying the ILT to the cylinder frame trajectory in (64), we obtain the incident-field frame trajectory $\mathbf{r}_c(t') = [x_c(t'), y_c(t'), z_c(t')]$ where

$$\begin{aligned} x_c(t') &= \mp\gamma a'\sin\left[\pm\omega'_c\left(t' - t'_g\right) + \phi'_k\right] + c\beta\gamma t' \\ y_c(t') &= \pm a'\cos\left[\pm\omega'_c\left(t' - t'_g\right) + \phi'_k\right] \\ z_c(t') &= z'_g + c\kappa'_z(t' - t'_g). \end{aligned} \tag{68}$$

Here, we refer to t' as a parameter along the 3-D trajectory $\mathbf{r}_c(t')$. For a given t', we identify, via the ILT, the corresponding incident-field frame time, t_c, as

$$t_c(t') = \gamma t' + \gamma\beta c a'\sin\left[\omega'_c\left(t' - t'_g\right) + \phi'_k\right]. \tag{69}$$

The CW trajectory in (68) is plotted in Fig. 6 for $\beta = 0.4$, $a' = 1$, and $\mathbf{k} = k\mathbf{u}_x$ for which $\kappa'_z = 0$ and the trajectory is a planar curve over the (x, y) plane. The projection over the (x, y) plane is periodic over the x-axis with a period of

$$\Delta x = v\Delta t, \quad \Delta t = \gamma\,\Delta t' = \gamma\, v\; 2\pi/\omega'_c \tag{70}$$

where ω'_c is given in (65). The velocity of the creeping potential over the trajectory $\mathbf{r}_c$ is given as

$$v_c(t') = \frac{d\mathbf{r}_c}{dt_c} = \frac{d\mathbf{r}_c}{dt'}\left(\frac{dt_c}{dt'}\right)^{-1}. \tag{71}$$

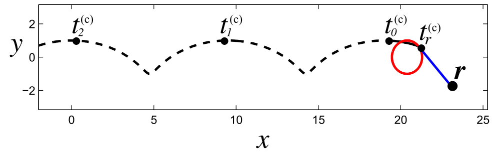

Fig. 6. Creeping wave trajectory in the incident-field frame. As the cylinder advances, the creeping waves follow the trajectory in (68). The cylinder is plotted in red at the radiation event in (77). The trajectory is corresponding to several creeping waves that are excited at $t_n^{(c)}$ when the incident ray is tangent to the cylinder.

By using (68) and (69) in (71), we obtain

$$v_c(t') = \frac{\left[\mp \gamma a'\omega_c' \cos\Phi_c(t') + c\beta, \mp a'\omega_c' \cos\Phi_c(t'), c\kappa_z'\right]}{\gamma\left[1 + c\beta a'\omega_c' \cos\Phi_c(t')\right]}. \tag{72}$$

Here, as in (68), t' is a parameter along the trajectory for which the corresponding physical time t_c is given in (69).

Next, we identify the cylinder frame creeping wave potentials events that correspond to a given *observation event* $(\mathbf{r}', ct')$. The potential in (61) consist of the ray field $G\left[k_\rho' L'^{(c)}(\rho')\right]$ that is emanating from the cylinder surface to the observation point. We denote the ray field *radiation event* in which the ray field is radiated from the cylinder surface by $(x_r'^{(c)}, y_r'^{(c)}, z_r'^{(c)}, ct_r'^{(c)})$. The ray field propagates a distance of $L'^{(c)}(\rho')$ at the speed of ck_ρ'/k' along the tangent trajectory from the radiation point over the cylinder surface to the observation point (see Fig. 5). Thus, the radiation event is evaluated by

$$\begin{aligned} x_r'^{(c)} &= \frac{a'}{\rho'^2}[a'y' \mp x'L'^{(c)}], \quad y_r'^{(c)} = \frac{a'}{\rho'^2}[\pm a'x' \pm y'L'^{(c)}] \\ z_r'^{(c)} &= z' - \kappa_z' c\left(t' - t_r'^{(c)}\right), \quad t_r'^{(c)} = t' - L'^{(c)}/\left(c\kappa_\rho'\right). \end{aligned} \tag{73}$$

Here, we have used the normalized wavenumbers in (63) and (65).

Next, we evaluate the cylinder frame event in which the creeping waves are excited. Since the creeping wave angular speed is ω_c' in (65), we evaluate the excitation (grazing) times of the mth potential that are denoted by $t_g'^{(c)m}$ via

$$t_{g\mp}'^{(c)m} = t_r'^{(c)} - \theta_\mp'^m/\omega_c' \tag{74}$$

where $\theta_\mp'^m$ is given in (59). Thus, the creeping wave is excited at the *grazing event* that is denoted by $(x_{g\mp}'^{(c)}, y_{g\mp}'^{(c)}, z_{g\mp}'^{(c)}$, *and* $ct_{g\mp}'^{(c)m})$ where

$$\begin{aligned} x_{g\mp}'^{(c)} &= \mp a' \sin\phi_k', \quad y_{g\mp}'^{(c)} = \pm a' \cos\phi_k' \\ z_{g\mp}'^{(c)m} &= z' - \kappa_z' c\left(t' - t_r'^{(c)} - t_{g\mp}'^{(c)m}\right). \end{aligned} \tag{75}$$

The radiation and grazing events can be mapped into the incident-field frame and be expressed in terms of the observation event (x, y, z, ct) via the ILT. For example, the radiation time that is denoted by $t_r^{(c)}$ is obtained by applying the ILT to the cylinder frame radiation event in (73), giving

$$t_r^{(c)} = \gamma\left[t' - \frac{L'^{(c)}(\rho')}{c\kappa_\rho} + \frac{\beta a'}{c\rho'^2}(a'y' \mp x'L'^{(c)}(\rho'))\right]. \tag{76}$$

By applying the LT in (5) to the observation event and inserting into (76), we obtain the expression for $t_r^{(c)}$ in terms of the incident-field frame observation event in the form

$$t_r^{(c)} = \gamma\left[\bar{x}(t) - \frac{\bar{L}^{(c)}(\mathbf{r}, t)}{c\kappa_\rho} + \frac{\beta a'}{c\bar{\rho}(t)^2}[a'\bar{x} - y\bar{L}^{(c)}(\mathbf{r}, t)]\right] \tag{77}$$

where $\bar{L}^{(c)}$ is given in (67).

Thus, the incident-field frame creeping wave potentials at the observation event (x, y, z, ct) consist of infinite contributions of creeping waves that were excited at the mth grazing event. These waves are radiated from the cylinder surface at the radiation event along the tangent ray trajectory from the cylinder surface at time $t_r^{(c)}$ to the observation point. This ray field arrives at the observation point at time t.

D. Low-Speed Approximation

In this section, we derive the *low-speed approximation* (LSA) of the scattered potentials for $\beta \ll 1$ ($v \ll c$). The scatterer shape in the incident-field frame is given by the ellipse $\gamma^2(x - \beta ct)^2 + y^2 = a'^2$. By applying a first-order approximation in β, $\gamma^2 = (1 - \beta^2)^{-1} \approx 1$ and the cylinder retains its cyclic form. Thus, we denote the radius as a $(= a')$.

LSAs of different quantities are obtained by applying the first-order approximation in β. By applying the LSA to ϕ_k' in (13) and for $\bar{\rho}(t)$ and $\bar{\varphi}(t)$ in (30) and (36), we obtain

$$\begin{aligned} \phi_k' &\approx \phi_k + \beta\Delta_{\phi_k}, \Delta_{\phi_k} = \sin\phi/\sin\theta_k \\ \bar{\rho}(t) &\approx \rho + \beta\Delta_\rho, \Delta_\rho = -ct\cos\phi \\ \bar{\varphi}(t) &\approx \varphi + \beta\Delta_\varphi, \Delta_\varphi = ct\sin\phi/\rho - \Delta_{\phi_k}. \end{aligned} \tag{78}$$

Here, all unprimed quantities are the corresponding *stationary* $(\beta = 0)$ analogs, i.e., $\phi_k = \phi_k'|_{\beta=0}$, etc. Note that the polar coordinates $(\bar{\rho}, \bar{\phi})$ deviate from the stationary ones linearly with ct, i.e., the LSA is valid for $\beta c|t|/\rho \ll 1$.

Next, we examine the reflection angle $\bar{\delta}$. By applying the first-order approximation to all quantities in (51) and collecting terms, we obtain $\bar{\delta} \approx \delta + \beta\Delta_\delta$ with

$$\Delta_\delta = \frac{\rho^2\cos(2\delta - |\phi|)\mathrm{sgn}(\Delta_\phi)\sin\phi\Delta_\phi + a\sin\delta\Delta_\rho}{2\rho^2\cos(2\delta - |\phi|) + a\rho\cos\delta} \tag{79}$$

where the stationary cylinder reflection angle δ is obtained by solving (51) with $\beta = 0$.

First, we examine the *reflected* potentials in (49). The LSA of *wave potentials* is carried out in the following manner: we sample all amplitudes at $\beta = 0$, and apply a first order approximation to the phase terms. This procedure yields

$$\begin{aligned} \Psi_{a/f}^{(r)}(\mathbf{r}, t) &\approx (-1)\sqrt{\frac{R^{(r)}}{L^{(r)} + R^{(r)}}}\Psi_{a/f}^0 \exp(-jk_z z)\exp(j\omega t) \\ &\quad \times \exp[-jk_\rho(L^{(r)} - a\cos\delta)]\exp(-j\beta\Delta_{\Psi^r}) \end{aligned} \tag{80}$$

where

$$\Delta_{\Psi^r} = L^{(r)}\Delta_{k_\rho} + k_\rho\Delta_{L^{(r)}} + a\sin\delta\Delta_\delta + kx - \Delta_\omega t \tag{81}$$

with

$$\Delta_{k_\rho} = -k\cos\phi_k,\ \ \Delta_\omega = -\omega\cos\phi_k\sin\theta_k$$
$$\Delta_{L^{(r)}} = \frac{2\rho\Delta_\rho - a^2\sin 2\delta\Delta_\delta}{2(L^{(r)} + a\cos\delta)} + a\sin\delta\Delta_\delta. \tag{82}$$

In (80), the stationary quantities $L^{(r)}$ and $R^{(r)}$ are obtained by setting $\beta = 0$ in their corresponding moving cylinder ones, i.e., $R^{(r)} = a\cos\delta/2$, etc.

Thus, the LSA reflected potentials consist of the stationary ones with the phase correction $\beta\Delta_{\Psi^r}$. In view of (81), it consists of corrections due to changes in k_ρ, $L^{(r)}$, and δ. The last two terms of βkx and $-\beta\Delta_\omega t$ are due to the first-order approximation of the time dilation in LT in (5) and the well-known (LSA) Doppler shift, respectively.

Next, we investigate the *creeping* wave potentials in (66). By applying the LSA, we obtain

$$\bar{l}^m_\mp(\mathbf{r},t) \approx l^m_\mp + \beta\Delta_{l^m},\ \ \bar{L}^{(c)}(\mathbf{r},t) = L^{(c)} + \beta\Delta_{L^{(c)}}$$
$$\Upsilon'_{a/f} \approx \Upsilon_{a/f} + \beta\Delta_\Upsilon \tag{83}$$

where

$$\Delta_{l^m} = a\left[\left(\frac{a}{\rho}\frac{\cos\phi}{\sqrt{\rho^2-a^2}} \mp \frac{\sin^2\phi}{\sqrt{\rho^2-x^2}}\right)ct \pm \Delta_{\phi_k}\right]$$
$$\Delta_{L^c} = -\rho ct\cos\phi/L^{(c)}, \quad \Delta_\Upsilon = 3\Upsilon_{a/f}\cos\phi_k/2\sin\theta_k. \tag{84}$$

By using (84) in (66), we approximate

$$\Psi^{(c)(\pm)}_{a/f(m)}(\mathbf{r},t) \approx \Psi^0_{a/f}D_{a/f}\exp(-jk_z z)\exp(j\omega t)G(k_\rho L^{(c)})$$
$$\times\exp\left[-jk_\rho\left(1+\Upsilon_{a/f}\right)l^m_\mp\right]\exp(-j\beta\Delta_{\Psi^{(c)}}) \tag{85}$$

where $D_{a/f}$ and $\Upsilon_{a/f}$ are the stationary ($\beta = 0$) analogs of (58), G is defined in (22) and

$$\Delta_{\Psi^{(c)}} = kx - \Delta_\omega t + (1+\Upsilon_{a/f})l^m_\mp\Delta_{k_\rho} + k_\rho l^m_\mp\Delta_\Upsilon$$
$$+ k_\rho(1+\Upsilon_{a/f})\Delta_{l^m} + L^{(c)}\Delta_{k_\rho} + k_\rho\Delta_{L^{(c)}}. \tag{86}$$

Thus, the LSAs of the creeping potentials consist of the stationary cylinder potentials with the phase correction $\beta\Delta_{\Psi^{(c)}}$. The first two terms in (86) have been discussed with connection to (81). The next three terms adjust the *creeping wave* phase to the slowly moving cylinder. These terms are due to the small changes in k_ρ, $\Upsilon_{a/f}$, and the distance $l^m_\mp$. The last two terms adjust the *radiation* phase from the radiation event to the observer. These terms are due to small changes in k_ρ and in the distance $L^{(c)}$.

VI. Conclusion

In this paper, we have presented the scattering of a TH PW by a moving PEC cylinder. We have obtained the exact and the asymptotic solutions for the fast cylinder in the incident-field frame where we have identified the scattered asymptotic wave as a combination of a shadowing, reflected, and creeping waves. An explanation to the apparent shift in the shadow width, casting direction, and also an expression to the reflection angles have been derived from the relativistic length contraction effect and casuality principles. We have discussed the creeping-wave phenomenon and mapped its excitation, radiation, and observation events. Finally, we have derived the closed-form expressions for the potentials in the low-speed regime and discussed the corresponding wave phenomena.

References

[1] G. L. James, *Geometrical Theory of Diffraction for Electromagnetic Waves*. London, U.K.: Peter Peregrinus, 1986.

[2] S. W. Lee and R. Mittra, "Scattering of electromagnetic waves by a moving cylinder in free space," *Can. J. Phys.*, vol. 45, no. 9, pp. 2999–3007, 1967.

[3] D. de Zutter and J. van Bladel, "Scattering by cylinders in translational motion," *IEE J. Microw. Opt. Acoust.*, vol. 1, pp. 192–196, Nov. 1977.

[4] D. de Zutter, "Fourier analysis of the signal scattered by three-dimensional objects in translational motion. I," *Appl. Sci. Res.*, vol. 36, pp. 241–256, Jul. 1980.

[5] D. de Zutter, "Fourier analysis of the signal scattered by three-dimensional objects in translational motion. II," *Appl. Sci. Res.*, vol. 36, pp. 257–269, Jul. 1980.

[6] P. de Cupis, G. Gerosa, and G. Schettini, "Gaussian beam diffraction by uniformly moving targets," *Atti Della Fondazione Giorgio Ronchi*, vol. 56, nos. 4–5, pp. 799–811, 2001.

[7] P. de Cupis, "Radiation by a moving wire-antenna in the presence of plane interface," *J. Electromagn. Waves Appl.*, vol. 14, no. 8, pp. 1119–1132, 2000.

[8] P. de Cupis, G. Gerosa, and G. Schettini, "Electromagnetic scattering by an object in relativistic translational motion," *J. Electromagn. Waves Appl.*, vol. 14, no. 8, pp. 1037–1062, 2000.

[9] P. de Cupis, P. Burghignoli, G. Gerosa, and M. Marziale, "Electromagnetic wave scattering by a perfectly conducting wedge in uniform translational motion," *J. Electromag. Waves Appl.*, vol. 16, no. 3, pp. 345–364, 2002.

[10] M. I. Demen and A. Alkumru, "Relativistic scattering of a plane-wave by a uniformly moving half-plane," *IEEE Trans. Antennas Propag.*, vol. 54, no. 11, pp. 3429–3440, Nov. 2006.

[11] P. de Cupis, "An analytical solution for electromagnetic wave scattering by multiple wedges," *Opt. Commun.*, vol. 261, no. 2, pp. 203–208, 2006.

[12] T. Danov and T. Melamed, "Spectral analysis of relativistic dyadic green's function of a moving dielectric-magnetic medium," *IEEE Trans. Antennas Propag.*, vol. 59, no. 8, pp. 2973–2979, Aug. 2011.

[13] T. Danov and T. Melamed, "2D relativistic longitudinal Green's function in the presence of a moving planar dielectric-magnetic discontinuity," *J. Opt. Soc. Amer. A, Opt. Image Sci.*, vol. 29, no. 3, pp. 285–294, 2011.

[14] R. Tuvi and T. Melamed, "Asymptotic analysis of plane wave scattering by a fast moving PEC wedge," *IEEE Trans. Antennas Propagat.*, vol. 65, no. 7, pp. 3638–3644, Jul. 2017.

[15] R. F. Harrington, *Time-Harmonic Electromagnetic Field*. New York, NY, USA: Wiley, 2001.

Eliran Mizrahi was born in Jaffa, Israel, in 1985. He received the B.Sc. degree *(magna cum laude)* in electrical engineering and the M.Sc. degree from the Ben-Gurion University of the Negev, Beersheba, Israel, in 2011 and 2012, respectively.

He is currently with the Israel Aerospace Industry, Ben-Gurion, Israel. His current research interests include analytic and numeric methods in wave theory, metamaterials, and electrodynamics.

Timor Melamed (M'17) was born in Tel-Aviv, Israel, in 1964. He received the B.Sc. degree *(magna cum laude)* in electrical engineering and the Ph.D. degree from Tel-Aviv University, Tel Aviv, in 1989 and 1997, respectively.

From 1996 to 1998, he was collaborated with the Professor L. B. Felsen held a postdoctoral position with the Department of Aerospace and Mechanical Engineering, Boston University, Boston, MA, USA. From 1999 to 2000, he was with the Odin Medical Technologies. He is currently with the Department of Electrical and Computer Engineering, Ben Gurion University of the Negev, Beersheba, Israel. His current research interests include analytic techniques in wave theory, transient wave phenomena, inverse scattering, and electrodynamics.